Available online at www.sciencedirect.com
ScienceDirect

International Journal of Mass Spectrometry 260 (2007) 90–101

International Journal of Mass Spectrometry

www.elsevier.com/locate/ijms

SIMS ion microscopy imaging of boronophenylalanine (BPA) and $^{13}C^{15}N$-labeled phenylalanine in human glioblastoma cells: Relevance of subcellular scale observations to BPA-mediated boron neutron capture therapy of cancer

Subhash Chandra*, Daniel R. Lorey II

Cornell SIMS Ion Microscopy Laboratory, Department of Earth and Atmospheric Sciences, Snee Hall, Cornell University, Ithaca, NY 14853, United States

Received 1 June 2006; received in revised form 30 August 2006; accepted 5 September 2006
Available online 26 September 2006

Abstract

p-Boronophenylalanine (BPA) is a clinically approved boron neutron capture therapy (BNCT) agent currently being used in clinical trials of glioblastoma multiforme, melanoma and liver metastases. Secondary ion mass spectrometry (SIMS) observations from the Cornell SIMS Laboratory provided support for using a 6 h infusion of BPA, instead of a 2 h infusion, for achieving higher levels of boron in brain tumor cells. These observations were clinically implemented in Phase II experimental trials of glioblastoma multiforme in Sweden. However, the mechanisms for higher BPA accumulation with longer infusions have remained unknown. In this work, by using $^{13}C^{15}N$-labeled phenylalanine and T98G human glioblastoma cells, comparisons between the ^{10}B-delivery of BPA and the accumulation of labeled phenylalanine after 2 and 6 h treatments were made with a Cameca IMS-3f SIMS ion microscope at 500 nm spatial resolution in fast frozen, freeze-fractured, freeze-dried cells. Due to the presence of the Na–K-ATPase in the plasma membrane of most mammalian cells, the cells maintain an approximately 10/1 ratio of K/Na in the intracellular milieu. Therefore, the quantitative imaging of these highly diffusible species in the identical cell in which the boron or labeled amino acid was imaged provides a rule-of-thumb criterion for validation of SIMS observations and the reliability of the cryogenic sampling. The labeled phenylalanine was detected at mass 28, as the $^{28}(^{13}C^{15}N)^-$ molecular ion. Correlative analysis with optical and confocal laser scanning microscopy revealed that fractured freeze-dried glioblastoma cells contained well-preserved ultrastructural details with three discernible subcellular regions: a nucleus or multiple nuclei, a mitochondria-rich perinuclear cytoplasmic region and the remaining cytoplasm. SIMS analysis revealed that the overall cellular signals of both ^{10}B from BPA and $^{28}CN^-$ from labeled phenylalanine increased approximately 1.6-fold between the 2 and 6 h exposures. However, the subcellular distribution of ^{10}B was different than the ^{28}CN in the mitochondria-rich perinuclear cytoplasmic region: ^{10}B was reduced in this region, but ^{28}CN was not. These observations indicate that: (i) a comparable higher accumulation of BPA and phenylalanine at 6 h versus 2 h plausibly represents a similar time-dependent entry mechanism through the plasma membrane in response to cellular requirements for the amino acid in glioblastoma cells and (ii) intracellular processes, especially those implicated with mitochondria, can plausibly recognize BPA as a different molecule than phenylalanine and may significantly differ in its sequestration and metabolism. For further understanding cell cycle influence on BPA accumulation, DNA-synthesizing S-phase cells were compared with non-S-phase cells. SIMS observations revealed that after 1 h exposure to BPA, S-phase cells contained elevated levels of ^{10}B in their nucleus in comparison to the nucleus of non-S-phase cells. Consequently, one reason that longer BPA exposures would increase its accumulation in most tumor cells will be the movement of the cell cycle through the S-phase. These observations suggest further cell cycle research in BPA-mediated BNCT and may have special significance for brain tumors since tumor cells are primarily the only cells in the brain with active proliferation characteristics. This study also shows the need for cryogenic sampling for subcellular measurements in BNCT, as even a brief thaw of frozen samples can result in gross redistribution of boron in subcellular compartments.

Keywords: BNCT; Imaging; Freeze-fracture; Brain tumor; Amino acid transport

---

1. Introduction

Thousands of people around the globe each year are diagnosed with the malignant brain tumor glioblastoma multiforme. Once diagnosed, the patient may live less than 1 year. Glioblas-

---

* Corresponding author. Tel.: +1 607 255 3884; fax: +1 607 254 4780.
E-mail address: sc40@cornell.edu (S. Chandra).

1387-3806/$ – see front matter © 2006 Elsevier B.V. All rights reserved.
doi:10.1016/j.ijms.2006.09.006

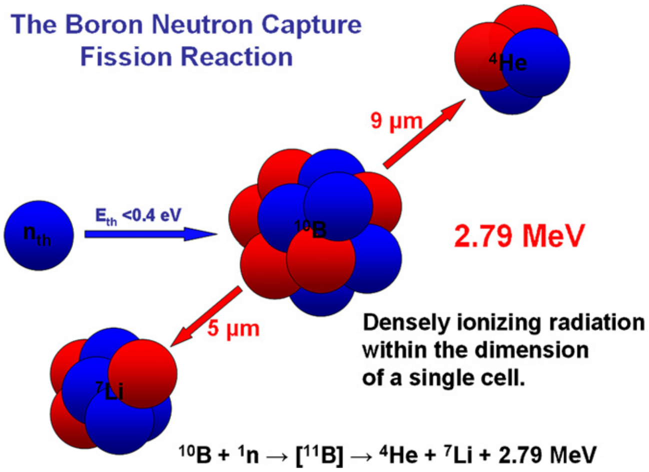

Fig. 1. Schematic of the boron neutron capture fission reaction. BNCT is based on the neutron capture reaction, $^{10}B(n,\alpha)^7Li$, where a ^{10}B atom captures a low-energy thermal neutron ($E_{th} < 0.4$ eV) and spontaneously decays to produce the linear recoiling particles ^{4}He (α particle) and ^{7}Li. In tissues, these particles have short penetration ranges, approximately the width of a single cell (5 μm for ^{7}Li and 9 μm for ^{4}He). The average linear energy transfer is high (^{7}Li, 162 keV/μm; ^{4}He, 196 keV/μm), which results in densely ionizing radiation restricted to the track of each particle.

toma multiforme is uniformly fatal and has no satisfactory treatment. Conventional surgical removal, generally limited to the main tumor mass, cannot remove the microscopic clusters of neoplastic cells that invade the surrounding normal brain far away from the main tumor mass. These infiltrating glioblastoma multiforme cells are responsible for the regrowth of the tumor [1]. Conventional radiotherapy cannot ablate these infiltrating cells in the normal brain [2], because the high radiation doses required to kill these cells would induce unacceptable levels of damage in the normal brain tissue [3].

Boron neutron capture therapy (BNCT) is a binary modality that has the potential for the treatment of many forms of cancers, such as glioblastoma multiforme brain tumors and melanomas [4–6]. The main requirements for this therapy are a selective targeting of tumor cells with sufficient quantities of ^{10}B atoms (15–30 μg/g or more) and their irradiation with low-energy thermal neutrons. BNCT is based on the neutron capture reaction, $^{10}B(n,\alpha)^7Li$, where a ^{10}B atom captures a low-energy thermal neutron ($E_{th} < 0.4$ eV) and spontaneously decays to produce the linear recoiling particles ^{4}He (α particle) and ^{7}Li (see Fig. 1). In tissues, these particles have short penetration ranges, approximately the width of a single cell (5 μm for ^{7}Li and 9 μm for ^{4}He). The average linear energy transfer is high (^{7}Li, 162 keV/μm; ^{4}He, 196 keV/μm), which results in densely ionizing radiation restricted to the track of each particle [7,8]. Cell killing is enhanced by intranuclear localization of ^{10}B, where radiation has a greater probability of damaging the DNA [9].

In theory, BNCT is potentially capable of killing individual cancer cells while sparing the healthy ones in the normal tissue. Consequently, knowledge of the microdistribution of ^{10}B from boronated drugs in cells of cancerous and normal tissues is of critical importance in BNCT [9]. An ideal drug would provide boron selectively to tumor cells and would not be toxic to cells in the normal tissue. Cell culture tumor models are ideally suited for understanding the mechanisms of boron delivery by BNCT agents [10,11]. Techniques capable of providing subcellular scale boron measurements are critically needed in BNCT [12–16]. The subcellular scale measurements require the use of reliable cryogenic sample preparations so that the native distribution of boron in subcellular compartments can be maintained during sampling. Ion microscopy, based on dynamic secondary ion mass spectrometry (SIMS), is ideally suited to BNCT due its high sensitivity and capabilities of: (i) subcellular spatially resolved 3D isotopic imaging with 500 nm spatial resolution, (ii) imaging of isotopically labeled molecules via the detection of the label and (iii) imaging of intracellular ^{39}K and ^{23}Na in the same cell for the validation of sample preparation and subcellular drug localization observations [12]. With over two decades of methodological developments at Cornell, SIMS ion microscopy has now become a versatile tool in BNCT for the evaluation of clinically approved and new BNCT agents [12].

The present study focuses on subcellular scale characterization of L-*p*-boronophenylalanine (BPA), a clinically approved BNCT agent, which is currently being used in clinical trials of various cancers including glioblastoma multiforme, melanomas and liver metastases [17]. Recent observations from our Cornell SIMS Ion Microscopy Laboratory provided support for a longer 6 h infusion of BPA for achieving higher levels of boron in tumor cells, as compared to a 2 h infusion, in both cell culture and animal models of glioblastoma multiforme [18–20]. The longer 6 h BPA infusion time supported by our SIMS observations was clinically implemented in Phase II experimental trials of glioblastoma multiforme in Sweden [17,21]. Longer BPA infusion protocols have now become an area of active research in BPA-mediated BNCT [17]. However, the mechanisms for higher boron accumulation in tumor cells with longer BPA infusions have largely remained unknown, and it is generally assumed that the amino acids are preferentially taken up by growing tumor cells. BPA may enter the cell via passive diffusion, L-amino acid transporter, or other method, and it may be taken up in malignant cells in larger amounts due to their increased metabolism [10,22]. Attempts have also been made for understanding the cell cycle dependence of BPA's accumulation in tumor cells [23,24].

In this work, by using $^{13}C^{15}N$-labeled phenylalanine and T98G human glioblastoma cells, a comparison between the ^{10}B-delivery by BPA and the accumulation of labeled phenylalanine was made with SIMS ion microscopy for understanding if the uptake characteristics of the boron analogue of the amino acid phenylalanine parallels those of phenylalanine itself. Furthermore, SIMS was also used for imaging the cell cycle associated differences in ^{10}B-delivery from BPA to glioblastoma cells.

2. Materials and methods

2.1. Materials

T98G human glioblastoma and LLC-PK1 renal epithelial pig kidney cell lines were obtained from the American Type Culture Collection (Manassas, VA, USA). ^{10}BPA (>95 at.% ^{10}B, L-isomer) was used as the fructose complex to increase its solubility in all experiments [25]. The ^{13}C, ^{15}N double-labeled phenylalanine amino acid (approximately 98% isotopic enrichment) was purchased from Cambridge Isotope Laboratories Inc. (Andover, MA, USA). Rhodamine 123 and 5-bromo-2′-deoxyuridine (BrdU) were purchased from Sigma (St. Louis, MO, USA). Latex beads (11 μm diameter) were purchased from Duke Scientific (Palo Alto, CA, USA). Polished high purity N-type semiconductor grade silicon wafers and germanium wafers were purchased from Silicon Quest International (Santa Clara, CA, USA).

2.2. Cell growth, drug treatments, cryogenic sample preparation

Cells from the T98G human glioblastoma cell line were propagated in Eagle's MEM with non-essential amino acids, 1.0 mM sodium pyruvate, Earle's BSS and 10% fetal bovine serum. The T98G cells were grown on the polished surface of high purity N-type semiconductor grade silicon pieces. An electrically conducting cell growth substrate is required for ion microscopy measurements since the sample is held at 4500 V in the sample chamber of the ion microscope. The silicon substrate is non-toxic to cells and has been used for SIMS studies of ion transport and drug localization. The silicon pieces (random shapes of about 1 cm^2 surface area) were sterilized prior to cell seeding. Each 60 mm plastic Petri dish used for cell growth contained four to six silicon substrates. The cells were seeded at a density of 250,000 cells per dish. Approximately 30,000 latex beads (11 μm diameter) were added to each Petri dish on the third day after cell seeding. These beads act as spacers in the cryogenic sandwich-fracture method described below for sample preparation. After the cells reached about 80% confluency on the silicon substrate, sister cells growing on different silicon substrates under identical conditions were divided and subjected to various treatments. The various treatments included: (i) exposure of cells to nutrient medium containing 110 μg/ml boron equivalent concentrations of BPA for 1, 2, 6, 8 and 16 h, (ii) 2 and 6 h exposures of cells to ^{13}C^{15}N-labeled phenylalanine in the same phenylalanine concentration as present in the 110 μg/ml boron equivalent of BPA (the cells for these treatments were grown on high purity germanium substrates because the silicon substrate interferes with mass $^{28}(^{13}C^{15}N)^-$ detection) and (iii) exposure of cells to 50 μM BrdU and 110 μg/ml boron equivalent of BPA for 1 h. In an additional treatments the T98G cells grown on silicon substrates were treated with rhodamine 123 for localization of mitochondria [26]. After the designated treatments, the cells were cryogenically prepared with a sandwich-fracture method [27]. The cells fractured at the apical membrane, produced by this method, are essentially the whole cells without the ectoplasmic face-leaflet of the plasma membrane [27,28]. The relatively large surface area of the silicon (or germanium) substrate generally contains multiple areas of fractured cells suitable for ion microscopy analysis. The cells were then freeze-dried at −90 °C overnight in a Tis-U-Dry Freeze-drier (FTS Systems Inc., Stone Ridge, NY, USA). The temperature of the sample stage of the freeze-drier was gradually increased to 40 °C to avoid any rehydration. The freeze-drier was vented to dry nitrogen, and the samples were quickly transferred to a desiccator. The samples were stored in the desiccator until optical and confocal microscopy and SIMS measurements were made.

2.3. Reflected light microscopy and confocal laser scanning microscopy measurements

The silicon (or germanium) substrates containing freeze-dried cells were transferred to an air-tight Teflon chamber with an optical window to avoid any rehydration during optical measurements [29]. An Olympus microscope with reflected light Nomarski optics was used for photographing the fractured freeze-dried cells. A Bio-Rad MRC 600/Zeiss Axiovert 10 confocal microscope was used for imaging of rhodamine 123 specific fluorescence in fractured freeze-dried T98G cells for mitochondrial localization. The freeze-dried cell matrix does not hinder fluorescence measurements with a confocal microscope [30] and allows one to evaluate the preservation of small organelles in individual cells for validation of cryogenic sampling and correlative drug localization.

2.4. Subcellular isotopic imaging with SIMS ion microscopy

A dynamic SIMS CAMECA IMS-3f ion microscope instrument (Paris, France) which provides a nominal spatial resolution of 500 nm was used for subcellular isotopic imaging studies [31]. Over its lifetime, the instrument has been upgraded and equipped with a primary beam mass filter, a 5f Hall Probe control chassis, and a Charles Evans and Associates model PC-1CS computer interface system for control of instrument operation. A 5.5 keV mass filtered primary ion beam of O_2^+ with a nominal beam current of 100 nA was focused to a spot size of about 60 μm in diameter when viewed at the surface of the sample. The primary ion beam was raster scanned over a 250 μm × 250 μm square region. A 60 μm contrast aperture was employed in the imaging mode throughout the study. The low-mass resolution SIMS ion microscopy imaging was done at a mass resolution of approximately 700. Prior to SIMS imaging, cells were coated with a thin layer of Au/Pd alloy to enhance their electrical conductivity, to minimize pre-sputtering time for signal stabilization, and to maintain an even electrical potential on the cell surface, especially for the initial analysis of the cell surface. In the positive secondary ion detection mode, images of isotopes with masses 10, 12, 23, 39 and 40 revealed the subcellular distribution of ^{10}B, ^{12}C, ^{23}Na, ^{39}K and ^{40}Ca, respectively. In the negative secondary detection mode, images of ^{12}C, ^{28}CN and ^{81}Br (or ^{79}Br) were recorded. In fractured freeze-dried cells, SIMS matrix effects (such as the practical ion yield variations and differential sputtering between the nucleus and the cytoplasm of individual cells) were not significant, and the secondary ion signals studied here did not reveal any significant mass interferences from polyatomic or hydrocarbon species [32]. Furthermore, analyses of fractured freeze-dried

T98G cells not treated with BPA did not show detectable ^{10}B signals.

2.5. High mass resolution SIMS analyses

High mass resolution analyses were performed for confirming the purity of ^{28}CN$^-$ signals in control cells and treatments with ^{13}C^{15}N-labeled phenylalanine. The instrumental conditions for such analyses have been described previously [33]. High mass resolution spectra of mass 28 were recorded by a digital slit imaging approach at a mass resolution of 4000. This resolution was sufficient for resolving three components in mass 28 negative secondary ion signals and unequivocally revealed the enhancement of the ^{28}CN$^-$ peak in cells treated with the ^{13}C^{15}N-labeled phenylalanine.

2.6. SIMS image quantification

Isotope images were digitized directly from the microchannel plate/phosphor screen assembly of the ion microscope using a slow scan charge-coupled device (CCD) camera (Photometrics; Tucson, AZ; Model CH220 CCD liquid-cooled camera head equipped with a Thomson-CSF TH7882 CDA CCD) and digitized to 14 bits per pixel with a Photometrics camera controller. Isotope image integration times varied according to their intensities. In general, in the positive secondaries the ^{39}K and ^{23}Na images were recorded for 0.4 s each. The ^{10}B, ^{12}C and ^{40}Ca images were recorded for 2 min. In the negative secondaries, the ^{12}C images were recorded for 10 s and ^{28}CN and ^{81}Br (or ^{79}Br) images were recorded for 2 min. A 2 min primary ion beam bombardment, under the experimental conditions, resulted in the erosion of an approximately 0.2 μm thick slice of the cell for integrating a desired SIMS image on the CCD camera. Within a single field of isotopic imaging, the variations in time of exposure for the isotope images were compensated for quantification in relation to the time of exposure of the ^{12}C image. Computer image processing was performed using DIP Station (Hayden Image Processing Group). Isotope images were quantified using relative sensitivity factors (RSF) to the cell matrix element ^{12}C$^+$ signals in the same spatial registration [34]. The absolute dry weight concentrations obtained by this method were converted into wet weight concentrations by assuming 85% cell water content. Analysis of variance (ANOVA) was used for testing the statistical significance of observations between different treatments.

3. Results and discussion

3.1. Morphological characterization of subcellular features in fractured freeze-dried T98G human glioblastoma cells by correlative optical and confocal laser scanning microscopy (CLSM) observations

T98G human glioblastoma cells are frequently multinucleated with irregularly shaped nuclei occupying a significant volume in the cell. A majority of these cells contain a well-defined characteristic organelle-rich perinuclear cytoplasmic region. This region is primarily occupied by mitochondria as is revealed by the correlative optical microscopy and CLSM analysis of the same fractured freeze-dried cells shown in Fig. 2. Fig. 2a shows a reflected light image of several multinucleated cryogenically prepared, apically fractured freeze-dried T98G cells. The boundaries of two representative nuclei have been outlined with dark dotted lines. The small rounded structures visible within each nucleus are nucleoli. Arrows in Fig. 2a indicate the discernible organelle-rich perinuclear region in each cell. As the live T98G cells were stained with rhodamine 123 for 30 min prior to cryogenic sampling, CLSM imaging of rhodamine 123 fluorescence from the identical fractured freeze-dried cells revealed the distribution of mitochondria in individual cells (Fig. 2b). The cell nuclei appear dark in the rhodamine 123 fluorescence image, while the brightly labeled mitochondria are distributed in the cytoplasm of each cell but with a much higher density in the organelle-rich perinuclear region identified in the optical image (compare the identical regions indicated by arrows in Fig. 2a and b). It should be noted that this is not a typical distribution of mitochondria in normal cell lines. In order to make sure that these observations are not some sort of artifact associated with the degradation of rhodamine 123 in the nutrient medium of T98G cells, co-cultures of T98G glioblastoma cells and a normal cell line, LLC-PK1 kidney cells, were grown together in the T98G nutrient medium on the silicon substrates. The co-cultures were treated with rhodamine 123

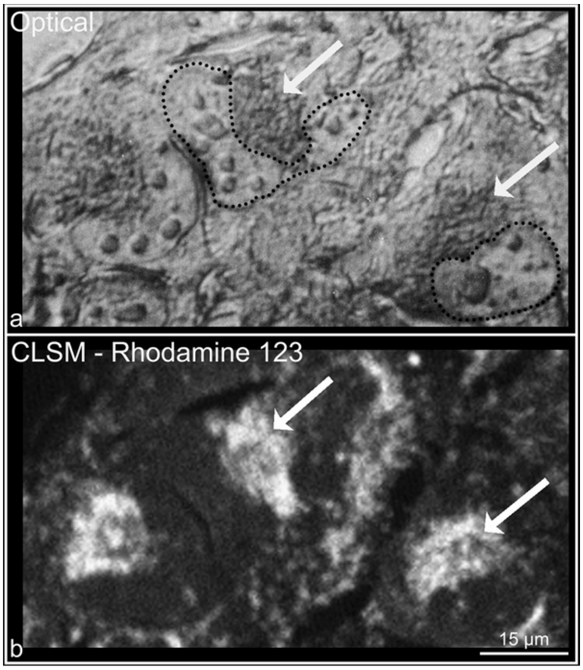

Fig. 2. Correlative reflected light microscopy and CLSM fluorescence imaging of rhodamine 123 in the same fractured freeze-dried T98G human glioblastoma cells. The optical image (a) shows several cells with irregular shaped nucleus also containing multiple nucleoli (dotted lines) and a perinuclear organelle-rich region (arrows) in each cell. The CLSM rhodamine 123 fluorescence image (b) revealing the distribution of mitochondria from the same cells shown in (a). The organelle-rich perinuclear region shows high density of mitochondria localization (arrows).

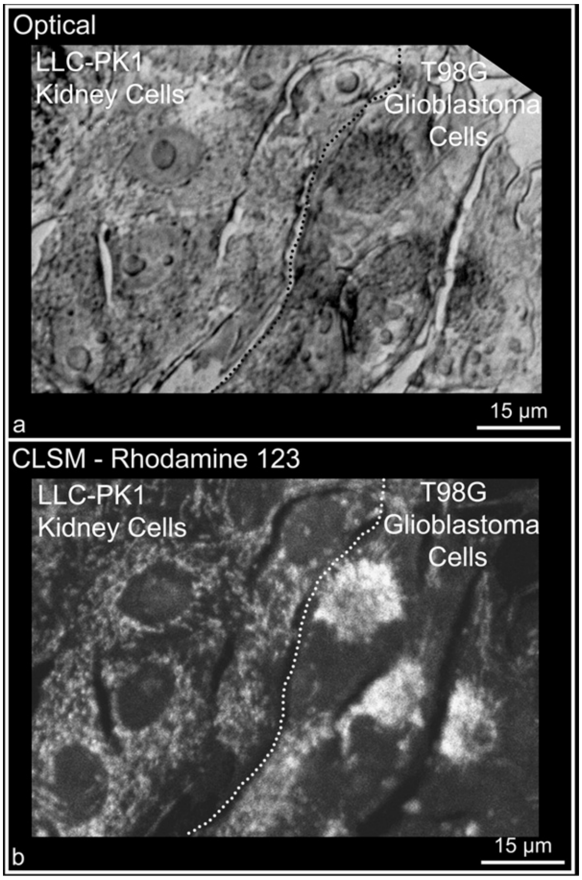

Fig. 3. Correlative reflected light microscopy (a) and CLSM fluorescence imaging of rhodamine 123 (b) in the same fractured freeze-dried co-cultures of LLC-PK1 pig kidney cells and T98G human glioblastoma cells. A dotted line shows the interface between the T98G cells mainly to right side and the LLC-PK1 cells to the left. The rhodamine 123 fluorescence distribution shows that mitochondria clusters in higher density in a perinuclear cytoplasmic region in T98G cells.

prior to cryogenic sampling. Fig. 3a and b show a correlative reflected light microscopy and CLSM imaging of rhodamine 123 fluorescence in fractured freeze-dried cells. A dotted line in these images shows the interface between the LLC-PK1 kidney cells and the T98G glioblastoma cells within the same field of view of fractured cells in this co-culture. The LLC-PK1 normal cell line lacks the characteristic perinuclear clustering of mitochondria and shows typical thread-like fluorescent structures throughout the cytoplasm. In contrast, the T98G cells reveal perinuclear clustering of mitochondria in the cytoplasm (Fig. 3a and b). These observations indicate a distinctive cell line characteristic of mitochondrial clustering in the perinuclear region of T98G glioblastoma cells. These observations are also consistent with a transmission electron microscopy study of T98G cells where clusters of mitochondria were observed in perinuclear regions [35]. A proper identification of these subcellular regions is important since they can be resolved with the spatial resolution of SIMS ion microscopy. Furthermore, these observations also indicate that the fractured freeze-dried cells contain well-preserved organelle level structural features for their SIMS analysis.

3.2. Quantitative subcellular SIMS imaging of time-dependent ^{10}B-accumulation from BPA in T98G human glioblastoma cells

For studying subcellular time-dependent ^{10}B-accumulation from BPA, T98G human glioblastoma cells were treated with 110 μg/ml boron equivalent of ^{10}BPA for 1, 2, 6, 8 and 16 h treatments and then cryogenically prepared for SIMS analysis. Fig. 4 shows an example of SIMS analysis of fractured freeze-dried T98G human glioblastoma cells after a 2 h treatment. The composite image shows a reflected light Nomarski photograph of several cells (Fig. 4a). The nucleus (or multiple nuclei) in each cell are discernible, and the smaller rounded structures inside the nuclear regions are nucleoli. The nuclear boundary in one cell is identified with a dotted line in Fig. 4a. The cell cytoplasm also shows a distinct perinuclear mitochondria-rich region which is identified by the arrow in the same cell in Fig. 4a. The other cells in the field of view also show these three subcellular compartments: the nucleus, mitochondria-rich perinuclear cytoplasm and the remaining cytoplasm. SIMS analysis of the same cells for ^{39}K, ^{23}Na, ^{40}Ca, ^{10}B and ^{12}C isotopic distributions are shown in Fig. 4b–f, respectively. Within an individual SIMS image, the level of brightness indicates the relative isotopic concentration. SIMS images represent the distribution of the total concentration of the analyte (both bound and free forms). Intracellular ^{39}K is distributed throughout the cells with no noticeable difference between nuclear and cytoplasmic compartments within a single cell. The ^{23}Na image of the same cells recorded for the same amount of time (0.4 s) as the potassium image reveals dim intensities and minor cell-to-cell differences. The cell peripheries show higher sodium signals due to adhering of the nutrient medium to the very edges of the cells and are ignored for quantitative calculations. The ^{40}Ca image from the same cells reveals the distribution of total calcium. The perinuclear cytoplasm (arrow) shows a higher calcium concentration than the nucleus in each cell. Indeed, the dim intensity nuclei in the calcium image correlate with the location of nuclei in the optical image (compare nuclear outlines in Fig. 4a and d). The ^{10}B image from the same cells reveals its subcellular distribution after 2 h exposure of T98G cells to ^{10}BPA (Fig. 4e). The mitochondria-rich perinuclear cytoplasmic region, indicated by the arrow in one cell, shows lower ^{10}B signals than the remaining cytoplasm or the nucleus. Overall, the ^{10}B is distributed throughout the cell with slight heterogeneity and in about comparable concentrations in the nucleus and the remaining cytoplasm (see nuclear boundary of the same cell identified in the boron image; Fig. 4e). The ^{12}C image shows nearly homogeneous carbon distribution in each cell (Fig. 4f).

Quantitative observations in the three discernible subcellular compartments of ^{10}B from BPA in all treatments are listed in Table 1. Intracellular concentrations of potassium and sodium are also listed for each treatment. Physiologically relevant levels of intracellular potassium and sodium provide confidence in the analysis of cryogenically prepared well-preserved healthy cells with K/Na ratios of approximately 10 (Table 1). The subcellular boron concentrations indicate that the perinuclear mitochondria-rich cytoplasmic region shows a consistent pattern of having

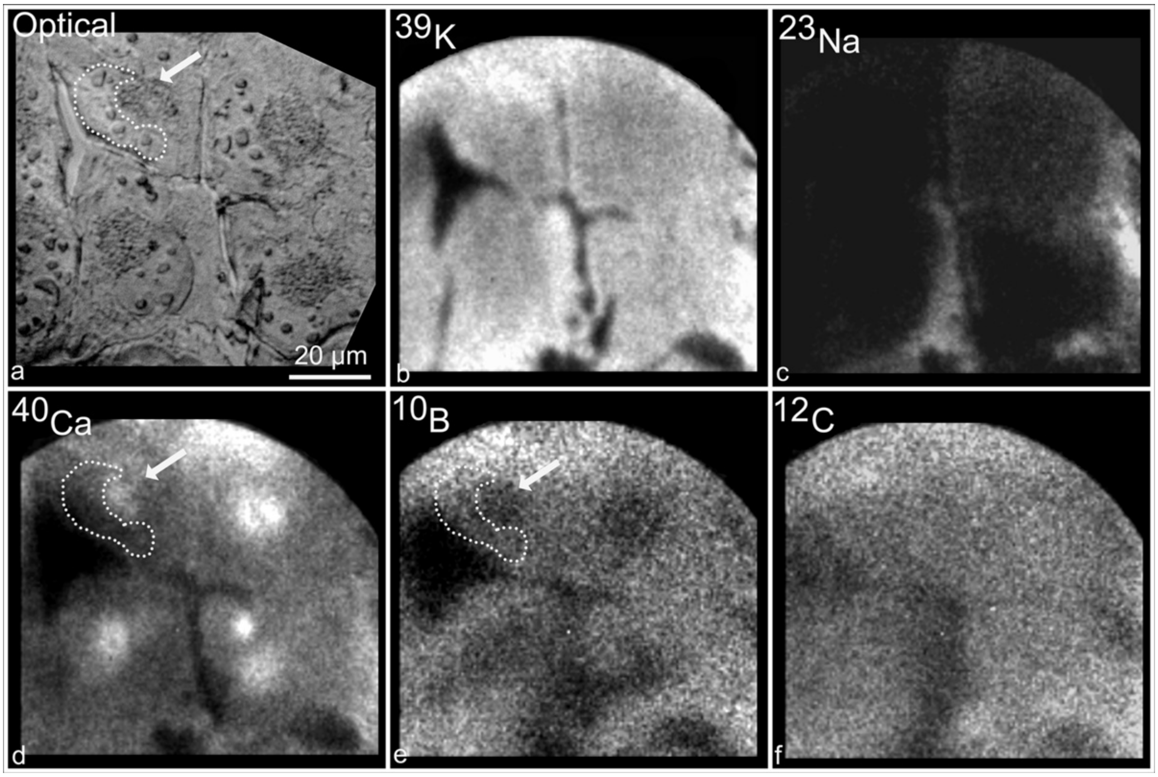

Fig. 4. SIMS isotope images of T98G human glioblastoma cells treated with 110 μg/ml boron equivalent of ^{10}BPA for 2 h. In the reflected light image (a) several fractured freeze-dried cells are shown with discernible nuclei (nucleus of one cell is shown with a dotted line) and a perinuclear mitochondria-rich cytoplasmic region (arrow). SIMS analysis of the same cells revealing subcellular isotopic distributions of ^{39}K (b), ^{23}Na (c), ^{40}Ca (d), ^{10}B (e) and ^{12}C (f) are shown. The areas within the dotted lines show the position of the nucleus and arrows indicate the mitochondria-rich perinuclear cytoplasmic region in SIMS images. Image integration times on the CCD camera for ^{39}K and ^{23}Na images were 0.4 s each and 120 s each for ^{40}Ca, ^{12}C and ^{10}B images.

a lower concentration of boron from BPA than the remaining cytoplasm or the nucleus in each treatment. The cell-to-cell difference in boron concentrations is also reflected in the standard deviation within each treatment. From the ^{10}B concentrations, it is also clear that a 6 h or longer BPA exposure significantly increases the intracellular accumulation of ^{10}B in all cellular regions of T98G human glioblastoma cells as compared to 1 and 2 h treatments (Table 1). For example, in 6 h versus 2 h BPA treatments, the boron accumulation was increased over 1.5-fold in cells (Table 1). The statistical analysis of the data indicates an initial period of boron accumulation which is not significantly different between 1 and 2 h of BPA exposure, and this BPA accumulation may represent both active and passive uptake mechanisms in glioblastoma cells. The significant increase ($P < 0.05$) in boron accumulation observed at 6 h and beyond reveals a plausible increase in the bound form of BPA, which is indicative of a cellular need for the amino acid. The higher standard deviation observed at 6 h further indicates a cell cycle-

Table 1
Time-dependent boron uptake in T98G human glioblastoma cells after treatment with 110 μg/ml boron equivalent of ^{10}BPA

Time of BPA exposure (h)	Cellular potassium (mM)	Cellular sodium (mM)	^{10}Boron[a] (wet weight, μg/g)		
			Nucleus	Mitochondria-rich perinuclear cytoplasm	Remaining cytoplasm
1	171 ± 20	14 ± 3	136 ± 55	109 ± 15	176 ± 57
2	163 ± 25	17 ± 4	191 ± 68	105 ± 21	141 ± 37
6	159 ± 19	15 ± 4	295 ± 120	185 ± 77	297 ± 140
8	179 ± 27	19 ± 6	295 ± 38	194 ± 38	341 ± 86
16	153 ± 23	17 ± 5	324 ± 73	202 ± 53	258 ± 92

Concentrations of potassium and sodium are expressed as mean ± S.D. on a cellular scale. Concentrations of boron are expressed as mean ± S.D. in three subcellular compartments: nucleus, mitochondria-rich cytoplasm and the remaining cytoplasm. SIMS observations were made in more than 20 cells in each treatment and similar patterns of boron accumulation were observed in 2 or more experiments. The absolute dry weight concentrations obtained by SIMS measurements from individual freeze-dried cells were converted into wet weight concentrations by assuming 85% cell water content.

[a] Statistical significance calculated from ANOVA indicated that all subcellular compartments revealed a similar pattern of change in boron accumulation upon increasing time of BPA exposure. The cells from the 1 and 2 h treatments were not significantly different from each other in boron accumulation. However, the cells in the 6, 8 and 16 h treatments showed significantly ($P < 0.05$) higher boron accumulation in all compartments as compared to the cells in the 1 and 2 h treatments.

dependent component of increased uptake of BPA in individual cells. This is further confirmed by the narrowing of the standard deviation at 8 and 16 h exposures due to movement of the cells through the cell cycle. Taken together, these observations indicate that the optimal accumulation time of boron from BPA is located between the 6 and 8 h time points for glioblastoma cells.

3.3. Subcellular SIMS imaging of $^{13}C^{15}N$-labeled phenylalanine accumulation in T98G human glioblastoma cells after 2 and 6 h exposures

Due to the clinical importance of the 2 h short exposure versus the 6 h long exposure of BPA for plausibly raising the boron content of tumor cells, ^{13}C, ^{15}N-labeled phenylalanine was used for understanding the similarities and differences in cellular uptake characteristics of labeled phenylalanine amino acid versus BPA after 2 and 6 h exposures in T98G cells. Fig. 5 shows chemical structures of boronophenylalanine and 98% enriched ^{13}C, ^{15}N uniformly labeled phenylalanine.

Mass 28 in the negative secondaries was chosen as a marker of the label due to its highly emissive nature for SIMS detection as the $^{28}(^{13}C^{15}N)^-$ molecular ion species. In 2 and 6 h treatments, a concentration of labeled phenylalanine identical to the concentration of phenylalanine present in 110 μg/ml boron equivalent of BPA was used. Fig. 6 shows SIMS imaging of the negative secondary ion signals of ^{12}C and ^{28}CN in fractured freeze-dried T98G cells. The top panels are from control cells not treated with the labeled amino acid (Fig. 6a and b), and the bottom panels are after a 2 h labeled phenylalanine treatment (Fig. 6c and d). The high sensitivity of dynamic SIMS can be appreciated in these measurements as the technique is capable of imaging the naturally abundant $^{28}CN^-$ signals even in control cells, which originate mainly from the combination of naturally abundant 1% ^{13}C isotope and 0.367% ^{15}N isotope. A direct comparison

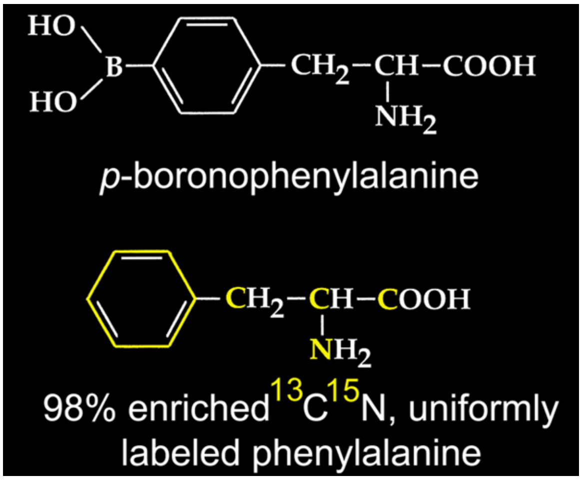

Fig. 5. Chemical structures of *p*-boronophenylalanine and $^{13}C^{15}N$-labeled phenylalanine.

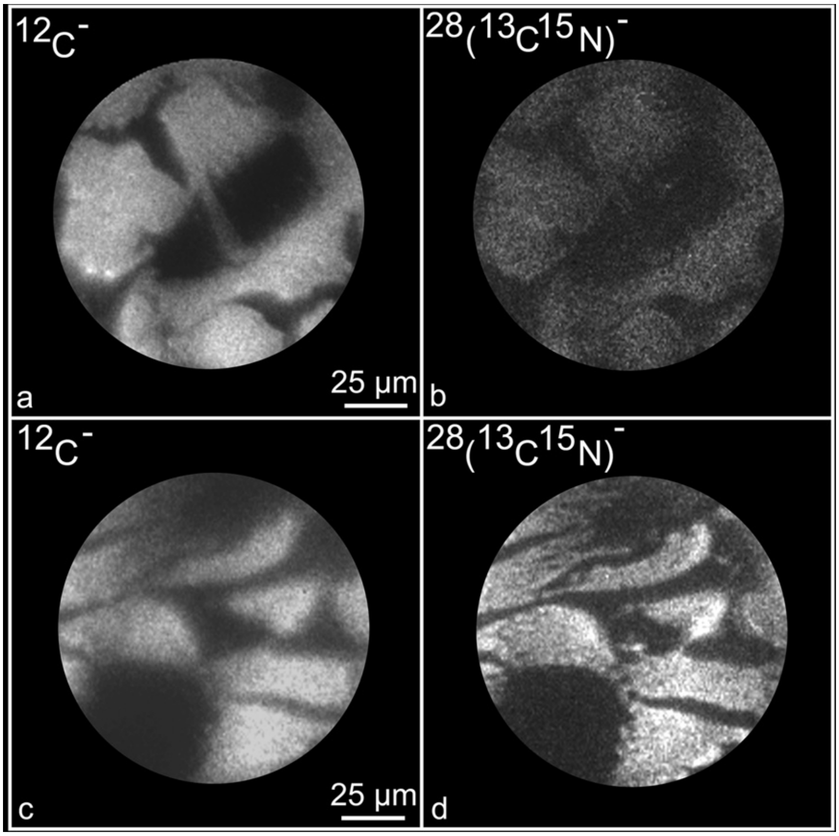

Fig. 6. SIMS imaging of $^{12}C^-$ and $^{28}(^{13}C^{15}N)^-$ signals in control T98G cells (a and b) and cells treated with $^{13}C^{15}N$-labeled phenylalanine for 2 h (c and d). The $^{28}(^{13}C^{15}N)^-$ signals in control T98G cells originate mainly from the combination of naturally abundant 1% ^{13}C isotope and 0.367% ^{15}N isotope. The $^{12}C^-$ image was integrated for 10 s and $^{28}(^{13}C^{15}N)^-$ for 120 s on the CCD camera.

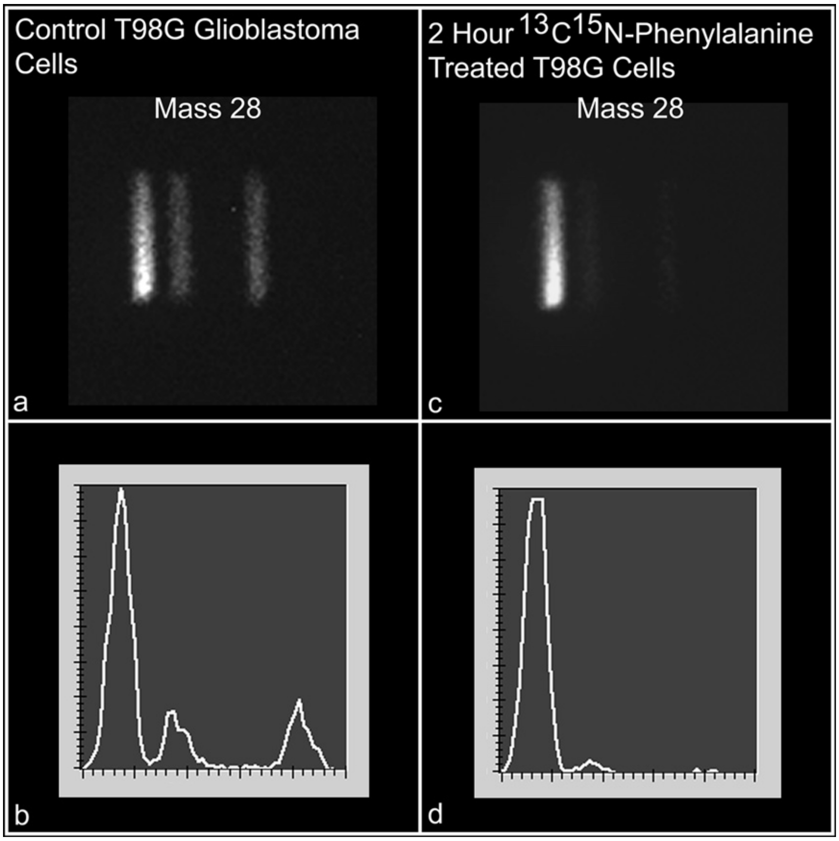

Fig. 7. SIMS high mass resolution spectra of mass 28 and the corresponding line scan from control T98G human glioblastoma cells (a and b) and cells treated with $^{13}C^{15}N$-labeled phenylalanine for 2 h (c and d). These observations represent a typical high mass resolution analysis (chosen from triplicate measurements). The three components in the cells represent $^{28}(^{13}C^{15}N)^-$ as the major component and, plausibly, $^{28}(^{12}C^{16}O)^-$ and $^{28}(^{12}C_2H_4)^-$ interfering components. The high mass resolution analysis conditions were able to separate all three components as illustrated in the figure. The $^{28}(^{13}C^{15}N)^-$ component of the line scans (b and d) has been scaled to the same extent in order to illustrate the enhancement of the component contributed by the labeled amino acid via the decrease of intensity of the interfering components.

of the control cells with cells treated for 2 h with the labeled phenylalanine shows enhancement of the $^{28}CN^-$ signals (compare Fig. 6b–d). This qualitative analysis shows the feasibility of imaging labeled phenylalanine with SIMS ion microscopy if the majority of the mass 28 signal originates from the $^{28}(^{13}C^{15}N)^-$ species and not from other interfering masses.

Fig. 7 shows a high mass resolution ($m/\Delta m \approx 4000$) analysis for a direct comparison of the various components in the mass 28 negative secondary ion signals in the control cells (Fig. 7a and b) and the cells treated for 2 h with labeled phenylalanine (Fig. 7c and d). The three component in the control cells potentially represent the $^{28}(^{13}C^{15}N)^-$, $^{28}(^{12}C^{16}O)^-$ and $^{28}(^{12}C_2H_4)$ species [36] and a representative line scan shows their relative fractions in the mass 28 image (Fig. 7a and b). The cells treated with $^{13}C^{15}N$-labeled phenylalanine for 2 h clearly show enhancement of the major component $^{28}(^{13}C^{15}N)^-$ in the cell matrix (Fig. 7c and d). These observations indicate that the labeled amino acid can be studied at mass 28 with SIMS ion microscopy in the routine low-mass resolution ion microscopy imaging mode of analysis.

Fig. 8 shows SIMS ion microscopy imaging of the labeled amino acid in glioblastoma cells after a 6 h exposure to $^{13}C^{15}N$-labeled phenylalanine. Individual fractured freeze-dried cells can be recognized with characteristic morphology in the reflected light Nomarski image (Fig. 8a). SIMS imaging of these cells for $^{40}Ca^+$, $^{28}(^{13}C^{15}N)^-$, $^{12}C^-$, $^{39}K^+$ and $^{23}Na^+$ distributions are shown in Fig. 8b–f, respectively. The cells show high K–low Na signals and concentrations indicative of healthy cells (Table 2). The $^{40}Ca^+$ image shows darker low-intensity nuclei in each cell. The mass $^{28}(^{13}C^{15}N)^-$ image reveals the distribution of the labeled amino acid (or its metabolite), which is distributed rather homogeneously throughout the cell and with no discernible difference in the mitochondria-rich perinuclear cytoplasmic region (Fig. 8c). These SIMS observations indicate plausible differences in the processing of phenylalanine from BPA, especially in mitochondria. It should be noted that SIMS imaging of the labeled phenylalanine this way cannot discriminate between its free pool or the mass 28 signals originating from the insertion of the labeled phenylalanine into proteins, peptides, etc.

A quantitative comparison of the ratio of $^{28}(^{13}C^{15}N)^-/^{12}C^-$ signals from individual T98G human glioblastoma cells between the 6 and 2 h treatments revealed a net increase of the label by nearly 1.6-fold (Table 2), which is almost the same increase as observed for boron from BPA between these time points (see Table 1). This remarkable SIMS observation indicates that both labeled phenylalanine and BPA may share common pathway(s) for entering the cell and shows the feasibility of using labeled

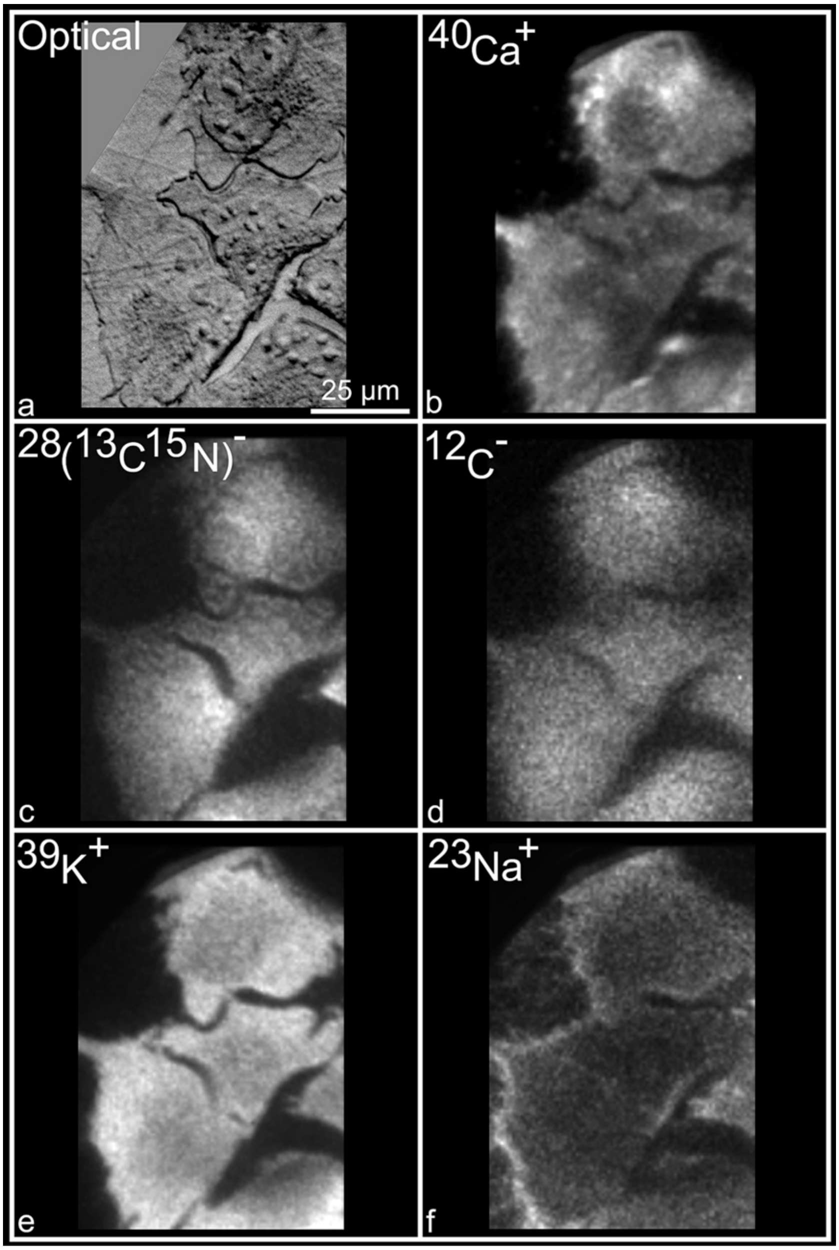

Fig. 8. SIMS isotope images of T98G human glioblastoma cells treated with $^{13}C^{15}N$-labeled phenylalanine for 6 h in the same concentration as the phenylalanine present in 110 μg/ml boron equivalent of ^{10}BPA. In the reflected light image (a) several fractured freeze-dried cells are shown with discernible nuclei and a perinuclear mitochondria-rich cytoplasmic region. SIMS analysis of the same cells revealing subcellular isotopic distributions of ^{40}Ca (b), $^{28}(^{13}C^{15}N)^-$ (c), ^{12}C (d), ^{39}K (e) and ^{23}Na (f) are shown. Image integration times on the CCD camera for the ^{40}Ca and $^{28}(^{13}C^{15}N)^-$ images were 120 s each. The $^{12}C^-$ image was integrated on the CCD camera for 10 s and ^{39}K and ^{23}Na images for 0.4 s each.

Table 2
SIMS imaging and quantitative comparison of the net accumulation of $^{28}(^{13}C^{15}N)^-$ label in T98G human glioblastoma cells treated with $^{13}C^{15}N$-labeled phenylalanine for 2 and 6 h treatments

Time of exposure to labeled phenylalanine (h)	Cellular potassium (mM)	Cellular sodium (mM)	Ratio of $^{28}(^{13}C^{15}N)^-/^{12}C^-$ SIMS signals from individual cells
2	168 ± 20	18 ± 6	0.0412 ± 0.0093
6	152 ± 23	16 ± 4	0.0696 ± 0.0173

The labeled amino acid was used in the same molar concentration of phenylalanine as present in 110 μg/ml boron equivalent of BPA. Concentrations of intracellular potassium and sodium are listed as mean ± S.D. The relative concentrations of the label are expressed as ratios of mass 28 $(^{13}C^{15}N)^-$ signals of individual cells to the corresponding $^{12}C^-$ signals within a treatment (mean ± S.D.). The data represent SIMS analysis of more than 35 cells in multiple imaging fields in each treatment from 2 experiments.

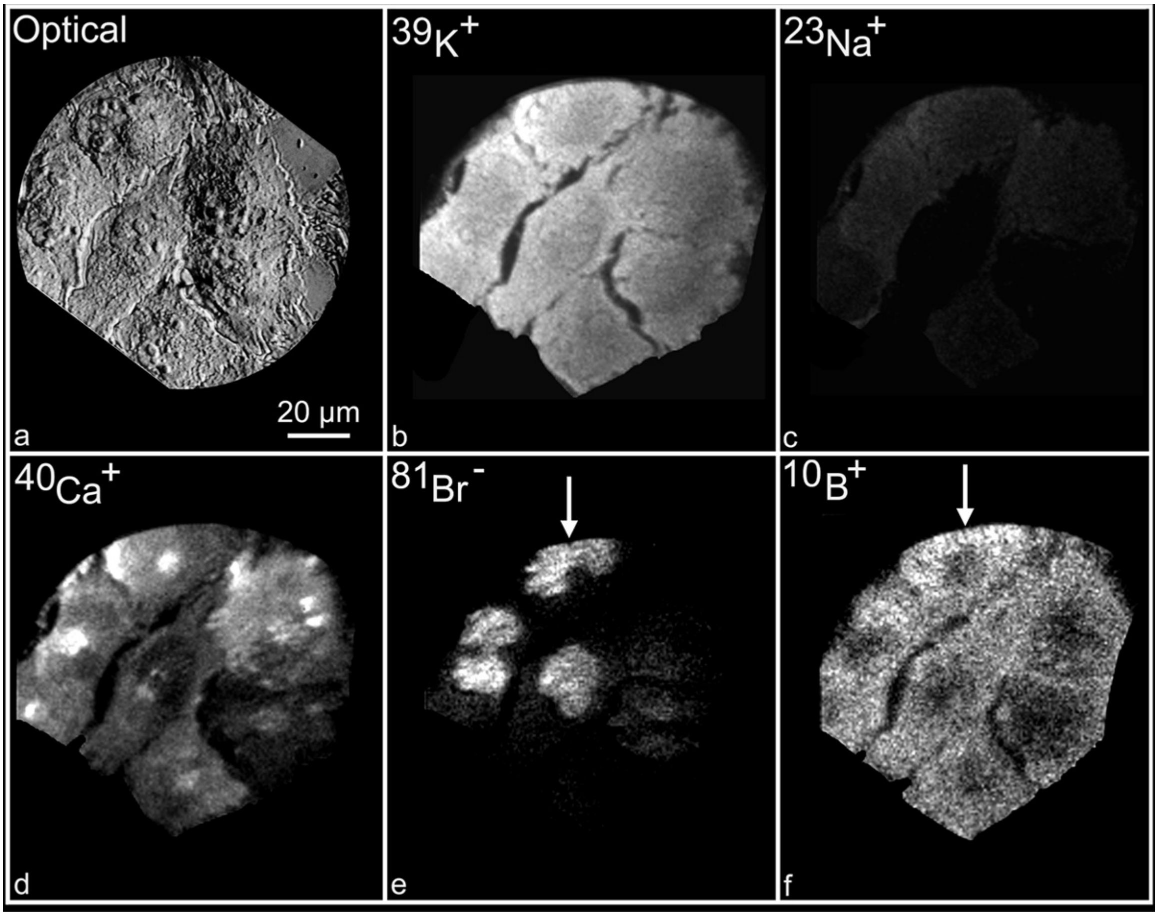

Fig. 9. Correlation of DNA-synthesizing S-phase cells with boron concentrations from BPA in asynchronously growing T98G human glioblastoma cells. The cells were treated with 50 μM BrdU and 110 μg/ml ^{10}B equivalent ^{10}BPA together for 1 h prior to cryogenic sample preparation. A reflected light Nomarski image shows several fractured freeze-dried cells (a). SIMS images of ^{39}K, ^{23}Na, ^{40}Ca, ^{81}Br and ^{10}B from the same cells are shown in (b–f), respectively. The S-phase cells show bright ^{81}Br signals in the nuclei of three cells (e, arrow indicates one such cell) which also contain slightly elevated levels of ^{10}B (f, arrow) compared to the non-S-phase cells in the field of view. Exposure times on the CCD camera for ^{81}Br, ^{10}B and ^{40}Ca images were 120 s each. The ^{39}K and ^{23}Na images were recorded for 0.4 s each.

compounds for unraveling the mechanistic aspects of BNCT agents.

3.4. *Direct imaging of BPA accumulation in DNA-synthesizing S-phase cells with SIMS*

Since many tumor cells may be actively involved in replicating their DNA, the evaluation of the targeting of the DNA-synthesizing S-phase versus the non-S-phase cells by BPA has remained an open question in BNCT, and only a few attempts have been made for observing the effect of cell cycle on BPA accumulation in tumor cells [23,24]. Fig. 9 shows an example that such measurements are directly amenable to SIMS analysis in cryogenically prepared cells. Bromodeoxyuridine (BrdU), being a thymidine analogue, provides a unique selectivity for targeting the nucleus of DNA replicating cells. This provides a novel strategy for correlation of S-phase cells with boronated drug accumulation in asynchronously growing cultures. Fig. 9 shows a direct SIMS ion microscopy approach for evaluating the efficiency of BPA for targeting S-phase cells. The cells were treated with 110 μg/ml boron equivalent of BPA and 50 μM BrdU for 1 h prior to cryogenic sampling. Fig. 9a shows the optical image of six fractured freeze-dried T98G human glioblastoma cells. SIMS analysis of the same cells for ^{39}K, ^{23}Na, ^{40}Ca, ^{81}Br and ^{10}B distributions are shown in Fig. 9b–f, respectively. Three cells on the left side are actively replicating their DNA, as indicated by the labeling of their nuclei by BrdU, as revealed in the ^{81}Br ion microscopy image (Fig. 9e). Remarkably, the ^{10}B signals from BPA in the S-phase glioblastoma cells are slightly elevated in their nuclei as compared to the nuclei of non-S-phase cells (Fig. 9f). Consequently, one reason that the longer BPA exposures would increase its accumulation in most tumor cells will be the movement of the cell cycle through the S-phase. These observations suggest further cell cycle research in BPA-mediated BNCT and may have special significance for brain tumors since tumor cells are primarily the only cells in the brain with active proliferation characteristics.

3.5. *The need for cryogenic sampling with validation of results for subcellular boron measurements in BNCT*

Throughout this work, the need for cryogenic sampling with validation of results is emphasized for subcellular measurements in BNCT. An example is shown here to show that gross redistribution of intracellular chemical composition and drug relocation may occur if frozen samples are thawed even briefly. In contrast to the SIMS observations shown above, if the silicon chips from the BPA-treated cells are taken out of the liquid nitrogen, thawed for a brief period of only 60 s at room temperature, and then put back in the liquid nitrogen for further cryogenic processing followed by freeze-drying, gross redistribution of not only intracellular K and Na, but also the ^{10}B subcellular signals from BPA is observed (Fig. 10). Fig. 10a shows a reflected light micrograph of such a briefly thawed specimen revealing nuclei of several T98G glioblastoma cells in the field of view. SIMS analysis of these cells for ^{40}Ca, ^{39}K, ^{23}Na and ^{10}B from BPA is shown in designated panels in Fig. 10b–e, respectively. It is clear that the cells now contain higher intracellular ^{23}Na than ^{39}K, and they no longer show the dim ^{40}Ca gradients in the nuclei. The ^{10}B from BPA has diffused throughout the cells because of the brief thaw, and the discernible low ^{10}B concentrations in the perinuclear mitochondria-rich region can no longer be recognized. This simple example conveys the message that subcellular measurements of boronated compounds in BNCT cannot be taken

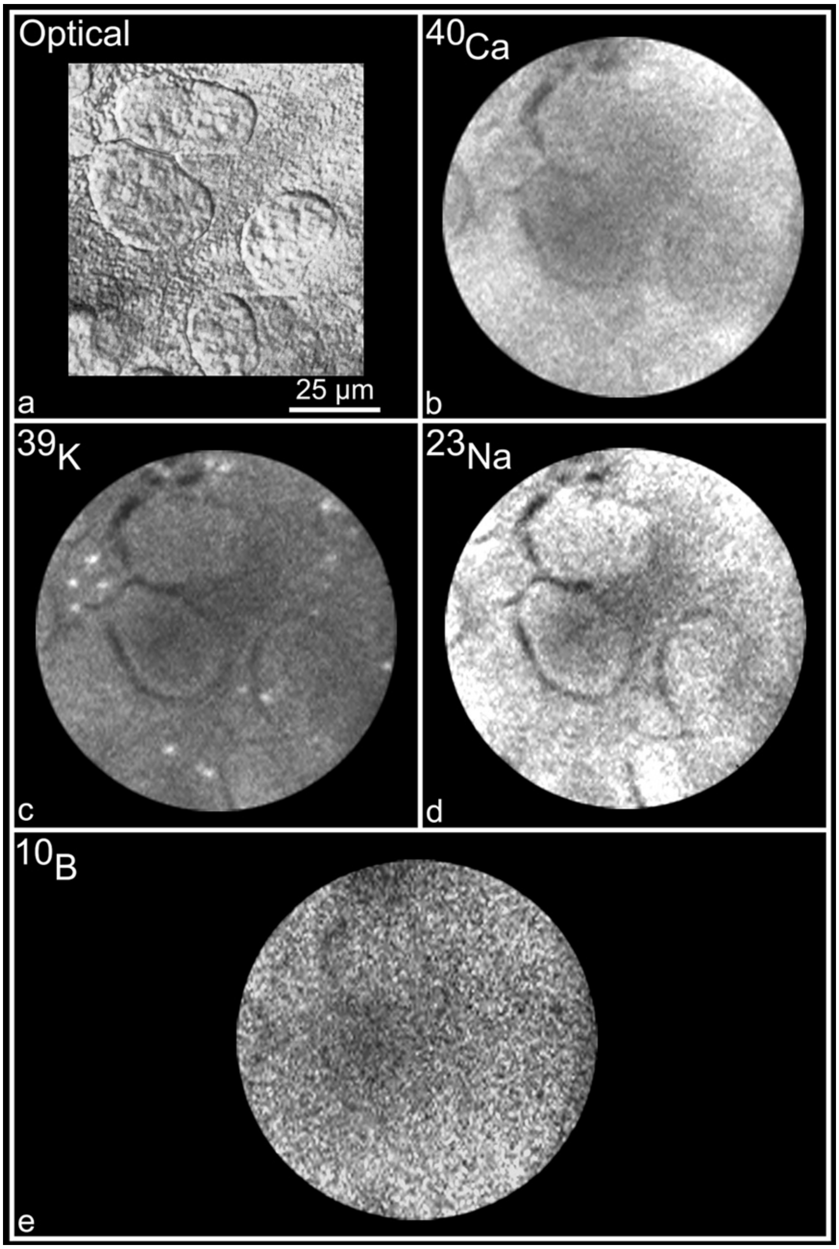

Fig. 10. An example of the effect of a brief thaw on frozen samples. SIMS isotope images of T98G human glioblastoma cells after a 1 h exposure of 110 μg/ml boron equivalent of ^{10}BPA and after a thaw of frozen samples for 60 s at room temperature are shown. In the reflected light Nomarski image of fractured, freeze-dried cells, nuclei of individual cells are discernible (a). SIMS analysis of the same cells revealing subcellular isotopic distributions of ^{40}Ca, ^{39}K, ^{23}Na and ^{10}B from ^{10}BPA are shown in designated panels (b–e). The thawing of samples has resulted in the gross redistribution of not only the intracellular chemical composition as reflected in ^{40}Ca, ^{39}K and ^{23}Na SIMS images but also the ^{10}B distribution from BPA. The ^{10}B and ^{40}Ca images were integrated on the CCD camera for 120 s and the ^{39}K and ^{23}Na were recorded for 0.4 s each.

lightly and must be validated by known markers of intracellular chemical composition or other suitable methods to prove their reliability.

4. Conclusions

Subcellular boron measurements are critically needed for understanding the mechanistic aspects of BNCT agents for boron delivery. SIMS ion microscopy studies of BPA and $^{13}C^{15}N$-labeled phenylalanine in cryogenically prepared cells showed a remarkable similarity of their increased accumulation in longer 6 h versus shorter 2 h exposures in T98G human glioblastoma cells. These observations indicate that BPA may enter the cell via pathways common to the amino acid phenylalanine. However, the processing of BPA may be quite different than phenylalanine, especially in the mitochondria of T98G cells. These observations are highly relevant to BNCT of brain tumors, where longer exposures of BPA can potentially enhance the boron partitioning of tumor cells to normal cells in the brain. This study also shows a direct approach for comparing boron targeting of S-phase cells with SIMS imaging after pulsing the cells with BrdU along with the boronated agent in question. These approaches will open new avenues of research in BNCT for the use of labeled molecules and the evaluation of the efficacy of new BNCT agents specifically designed to target the DNA-synthesizing cells. Finally, the study emphasizes the need and value of cryogenic sample preparation for subcellular boron measurements in BNCT.

Acknowledgments

This research was supported by the Biological and Environmental Research Program (BER), U.S. Department of Energy, Grant No. DE-FG02-91ER61138. We are thankful to Professor Watt W. Webb and Professor Warren Zipfel for the use of their NIH/NSF Developmental Resource for Biophysical Imaging Opto-electronics at Cornell in culturing cells for this study.

References

[1] P.C. Burger, P.J. Dubois, S.C. Schold Jr., K.R. Smith Jr., G.L. Odom, D.C. Crafts, F. Giangaspero, J. Neurosurg. 58 (1983) 159.
[2] A.C. Halperin, P.C. Bruger, D.E. Bullaard, Int. J. Radiat. Oncol. Biol. Phys. 15 (1988) 505.
[3] F.J. Sullivan, L.L. Hersher, J.A. Cook, J. Smith, S.M. Steinberg, A.H. Epstein, E.H. Oldfield, T.E. Goffman, T.J. Kinsella, J.B. Mitchell, E. Glastein, Int. J. Radiat. Oncol. Biol. Phys. 30 (1994) 583.
[4] R.F. Barth, A.H. Soloway, R.G. Fairchild, Sci. Am. 263 (1990) 100.
[5] J.A. Coderre, G.M. Morris, Radiat. Res. 151 (1999) 1.
[6] W.H. Sweet, N. Engl. J. Med. 245 (1951) 875.
[7] R.F. Barth, A.H. Soloway, R.G. Fairchild, R.M. Brugger, Cancer (Phila.) 70 (1992) 2995.
[8] T. Kobayashi, K. Kanda, Radiat. Res. 91 (1982) 77.
[9] D. Gabel, S. Foster, R.G. Fairchild, Radiat. Res. 111 (1987) 14.
[10] J. Capala, J.S. Makar, J.A. Coderre, Radiat. Res. 146 (1996) 554.
[11] P. Panov, Y. Salomon, G.W. Kabalka, P. Bendel, Radiat. Res. 154 (2000) 104.
[12] S. Chandra, D.R. Smith, G.H. Morrison, Anal. Chem. 72 (2000) 104A.
[13] M. Fartmann, C. Kriegeskotte, S. Dambach, A. Wittig, W. Sauerwein, H.F. Arlinghaus, Appl. Surf. Sci. 231–232 (2004) 428.
[14] J. Michel, W. Sauerwein, A. Wittig, G. Ballossier, K. Zierold, J. Microsc. 210 (2003) 25.
[15] T.U. Probst, Fresenius J. Anal. Chem. 364 (1999) 391.
[16] G.R. Solares, R.G. Zamenhof, Radiat. Res. 144 (1995) 50.
[17] R.F. Barth, J.A. Coderre, G.H. Vicente, T.E. Blue, Clin. Cancer Res. 11 (2005) 3987.
[18] S. Chandra, G.W. Kabalka, D.R. Lorey II, D.R. Smith, J.A. Coderre, Clin. Cancer Res. 8 (2002) 2675.
[19] S. Chandra, D.R. Lorey II, D.R. Smith, Radiat. Res. 157 (2002) 700.
[20] D.R. Smith, S. Chandra, R.F. Barth, W. Yang, D.D. Joel, J.A. Coderre, Cancer Res. 61 (2001) 8179.
[21] J. Capala, B. H-Stenstam, K. Skold, P.M. Rosenschold, V. Giusti, C. Persson, E. Wallin, A. Brun, L. Franzen, J. Carlsson, L. Salford, C. Ceberg, B. Persson, L. Pellettieri, R. Henricksson, J. Neurooncol. 62 (2003) 135.
[22] A. Wittig, W.A. Sauerwein, J.A. Coderre, Radiat. Res. 153 (2000) 173.
[23] R. Kubota, S. Yamada, K. Ishiwata, M. Tada, T. Ido, K. Kubota, Br. J. Cancer 67 (1993) 701.
[24] F. Yoshida, A. Matsumura, Y. Shibata, T. Yamamoto, H. Nakauchi, M. Okumura, T. Nose, Cancer Lett. 187 (2002) 135.
[25] J.A. Coderre, T.M. Button, P.L. Micca, C. Fischer, M.M. Nawrocky, H.B. Liu, Int. J. Radiat. Oncol. Biol. Phys. 30 (1994) 643.
[26] L.V. Johnson, M.L. Walsh, L.V. Chen, Proc. Natl. Acad. Sci. U.S.A. 77 (1980) 990.
[27] S. Chandra, G.H. Morrison, C.C. Wolcott, J. Microsc. (Oxford) 144 (1986) 15.
[28] S. Chandra, G.H. Morrison, J. Microsc. (Oxford) 186 (1997) 232.
[29] S. Chandra, G.H. Morrison, Biol. Cell. 74 (1992) 31.
[30] S. Chandra, E.P.W. Kable, G.H. Morrison, W.W. Webb, J. Cell Sci. 100 (1991) 747.
[31] R. Castaing, G. Slodzian, J. Microscopie (Paris) 1 (1962) 395.
[32] S. Chandra, W.A. Ausserer, G.H. Morrison, J. Microsc. (Oxford) 148 (1987) 223.
[33] S. Chandra, G.H. Morrison, J. Microsc. (Oxford) 188 (1997) 182.
[34] W.A. Ausserer, Y.-C. Ling, S. Chandra, G.H. Morrison, Anal. Chem. 61 (1989) 2690.
[35] M. Weller, S. Winter, C. Schmidt, P. Esser, A. Fontana, J. Dichgans, P. Groscurth, Int. J. Cancer 73 (1997) 707.
[36] R.A. Burdo, G.H. Morrison, Materials Science Center Report #1670, Cornell University, Ithaca, NY, 1971, p. 1.